Nuclear Inst. and Methods in Physics Research, A 985 (2021) 164662

Contents lists available at ScienceDirect

Nuclear Inst. and Methods in Physics Research, A

journal homepage: www.elsevier.com/locate/nima

Development of a passive gold-foil Nested Neutron Spectrometer to validate the active current-mode He-3 measurements in a high neutron fluence rate radiotherapy environment

Felix Mathew [a,*], Cornelia Chilian [b], Logan Montgomery [a], John Kildea [a]

[a] Medical Physics Unit, McGill University, Montreal, QC, H4A3J1, Canada
[b] Department of Engineering Physics, Polytechnique Montreal, Montreal, QC, H3T1J4, Canada

ARTICLE INFO

Keywords:
Neutrons
Radiotherapy
Nested Neutron Spectrometer
Passive Spectrometer
Gold foil

ABSTRACT

Nested Neutron Spectrometers^{TM} (NNS) can be used to measure neutron fluence rate spectra under diverse circumstances with a working principle similar to Bonner sphere systems. Conventionally, the NNS consists of an active-readout He-3 detector core and concentric moderator shells. In environments where the neutron fluence rate exceeds $\backsim 10^4$ neutrons/s, these spectrometers may be operated in a current-mode to avoid the effects of pulse pile-up and deadtime. A current-to-pulse conversion factor is used to convert current-mode measurements to pulse-mode. However, the conversion factor can only be directly calibrated under low-flux conditions due to the pulse pile-up in high-flux situations. In order to have confidence in the use of the conversion factor in high neutron fluence rate environments such as in high-energy radiotherapy, its use must be experimentally validated. To perform this validation, we developed a passive-readout NNS with gold activation foils. Our work included the generation of system response functions using the Monte Carlo toolkit, GEANT4, and an experimental workflow. The passive NNS and the active NNS were then used to measure the secondary neutron fluence rate spectra produced by a Varian TrueBeam^{TM} STx linac under identical experimental conditions. We found that the spectrum obtained using the active NNS agreed well with that obtained using the passive NNS within uncertainties. This serves as validation of the use of the current-mode of the active NNS in the high neutron fluence rate conditions encountered in radiotherapy.

1. Introduction

Modern radiotherapy techniques utilize various types of ionizing radiation spanning a wide energy range [1]. High-energy radiation is often necessary to treat deeply-seated tumours in order to adequately deliver the prescribed dose. In high-energy photon radiotherapy ($\gtrsim$ 10 MV), secondary neutrons are generated as an unwanted byproduct through photonuclear reactions in the materials that the photon beam encounters [2–5]. These neutrons contribute to the out-of-field dose received by the patient and thereby pose an iatrogenic risk for carcinogenesis [6–8]. Since the neutron's carcinogenic potential has been shown to vary with energy [9,10], it is essential to determine the neutron fluence rate spectrum experienced by the patient inside the radiotherapy bunker in order to properly assess the carcinogenic risk involved.

The Nested Neutron Spectrometer™ (NNS, Detec Inc., Gatineau, QC, Canada) [11] is one of many types of neutron spectrometers [12–14] that are used to measure neutron spectra, including in the high-energy radiotherapy environment. The NNS comprises a He-3 thermal neutron detector embedded in concentric cylindrical-moderator shells (Fig. 1) that can be assembled in multiple configurations of various moderator thicknesses. By varying the thickness of the moderator, the user can selectively moderate the incoming neutron energy to the sensitive range of the He-3 detector. This spectrometer with the He-3 detector core, which gives an immediate electronic readout, is henceforth referred to as the active NNS.

The He-3 detector of the active NNS can be operated in either pulse-mode or current-mode. In pulse-mode, the He-3 detector works as a proportional counter and is connected to a multi-channel analyzer (MCA) that counts the number of ionization events (pulses) originating in the detector's sensitive volume [15]. However, when the count-rate exceeds $\backsim$10,000 counts/s, pulse-mode breaks down due to pulse-pileup and increased dead-time [11]. Hence, in radiotherapy environments, where the neutron count-rate typically exceeds 10,000 counts/s, the active NNS must be operated in current-mode [15], similar to the method described by Hagiwara et al. in 2011 [16]. In current-mode, the He-3 detector acts as an ionization chamber and neutron-induced current is measured using an electrometer.

* Corresponding author.
E-mail address: felix.mathew@mail.mcgill.ca (F. Mathew).

https://doi.org/10.1016/j.nima.2020.164662
Received 6 June 2020; Received in revised form 11 September 2020; Accepted 14 September 2020
Available online 18 September 2020
0168-9002/

Fig. 1. Top-view of the Nested Neutron Spectrometer's cylindrical moderator shells and lids.

The current measurement may be converted to an equivalent pulse-rate using a conversion factor provided by the vendor and previously confirmed experimentally by our group [15]. This conversion factor is the ratio of the pulse-rate and the current for the same measurement conditions and was obtained by calibrating the detector using the low neutron fluence rate Am-Be reference source [17,18] at the Ionizing Radiation Standards Laboratory of the National Research Council of Canada. However, it is not possible to demonstrate directly that this conversion factor, which was determined in a low flux environment, is applicable in the high flux environment encountered in radiotherapy. Previously we performed a coarse validation of the NNS at high neutron fluence rate through comparison of measured spectra with Monte Carlo simulated spectra [15]. While we observed relatively good agreement, this in-silico approach could not completely substitute experimental validation at high flux due to the limitations of modelling such a complex system (physics models, linac geometry, bunker geometry, etc.).

In the work reported on here, we performed the validation indirectly, by developing a passive NNS system wherein the active He-3 detector was replaced with gold activation foils, which do not suffer from pulse-pile up or dead-time complications [19]. Activation foil-based spectrometry is widely reported in the literature and the use of various foil materials has also been well assessed [20–24]. Indeed, gold foils have been used extensively for neutron studies with other spectrometers, including the well-known Bonner Sphere Spectrometer [19,25–28]. This manuscript describes how we developed a passive NNS and used it to experimentally validate the current-mode of an active NNS in the high flux radiotherapy environment.

2. Materials and methods

2.1. Operation of the active NNS

The basic operational details of the active NNS can be found in our previously-published work [15,29]. Only the experimental details specific to this work are included in this manuscript.

The current-mode operation of the active NNS requires an electrometer to read out the neutron-induced current produced in the He-3 detector during an irradiation procedure. Note that the He-3 detector is sensitive to both neutrons and photons and, thus, the photon contribution to the measurement must be removed. As described in our previous work [15], this is done by acquiring analogous NNS measurements with a neutron-insensitive He-4 detector and subtracting the resulting charge or current from the He-3 result. The neutron current thus obtained can then be converted to an equivalent neutron pulse-rate using the vendor-provided conversion factor.

In order to determine the neutron fluence rate spectrum using the neutron pulse-rate data, one must have prior knowledge about the response of the spectrometer system used. For the active NNS, these response functions were generated and provided by the vendor [11]. Together with the response functions and an initial guess spectrum, the measured current values can be unfolded to produce the neutron fluence rate spectrum.

To obtain an active NNS spectrum, we irradiated an active NNS, obtained a set of neutron pulse-rates by converting the measured set of neutron currents using the conversion factor, and unfolded the neutron fluence rate spectrum using our previously-published unfolding algorithm [30].

2.2. Development of the passive NNS

To build a novel passive NNS we replaced the active He-3 detector core of an active NNS with passive gold foils. We opted to use gold foils after considering our experimental requirements, particularly (i) high thermal neutron sensitivity to detect thermalized neutrons at the centre of the moderators, and (ii) moderate half-life (∽2.7 days) that is neither too short nor too long. A 99.9% pure gold-foil (^{197}Au) disc (8 mm radius, 0.1 mm thick and 19.3 g cm^{-3} density) was placed perpendicular to the cylindrical axis of the NNS at the geometric centre of the moderator shells, and sandwiched by two cylindrical polyoxymethylene inserts custom-machined for the passive NNS. A side-by-side comparison of the active and passive systems for a single moderator configuration is shown in Fig. 2.

2.3. Generation of the passive NNS response functions

The response function of a system is essentially a map that connects the output of the system to its input parameters. In the context of the NNS, the response functions relate the neutron-induced measurements to the neutron fluence rate at the point of measurement. We generated the response functions of the passive NNS using Monte Carlo simulations built in GEANT4 (version 10.4, patch-2) [31–34]. Our passive NNS was modelled according to its physical dimensions and materials for all moderator configurations and therefore the model takes into account the neutron self-shielding and other geometry dependencies of the gold foil. In our simulations, neutron transport was nominally handled by the QGSP_BIC_HP high-precision neutron physics model, which includes the G4NDL neutron cross-section library (i.e standard ENDF-6 data [35] in GEANT4 compatible format) up to 20 MeV [36]. However, in 2014, Mendoza et al. demonstrated the necessity of using an accurate model for the thermal neutron scattering [37] and its significance on the simulation's outcome. Hence, we modified the QGSP_BIC_HP model to include the thermal neutron elastic scattering data below 4 eV.

With the General Particle Source (GPS) tool, neutron sources were randomly distributed on a cylindrical surface that encapsulated the biggest moderator of the passive NNS configuration in each simulation. From this source surface, 10^7 monoenergetic neutron tracks were made to originate from random directions to ensure an isotropic neutron field at the spectrometer surface.

The passive NNS response was defined as the number of neutron capture interactions per unit neutron fluence [38] and per unit mass of the gold foil. For each moderator configuration, the number of neutron capture interactions in the gold foil was scored with the spectrometer materials in place. A separate set of simulations was used to score the neutron fluence at the location of the gold foil with all the spectrometer materials replaced by air.

Consistent with the active NNS, the response of the passive NNS was determined for 52 discrete energies, logarithmically spaced from 1 meV to 16 MeV, for each detector configuration. Two variance reduction techniques, Geometric Splitting and Russian Roulette [39], were implemented in the simulation using the Importance Sampling technique of GEANT4 to increase the simulation efficiency [40]. The complete set of simulations required to generate all eight response functions of the

(a) (b) (c)

Fig. 2. (a) Single-shell configuration of the active NNS; (b) Photo of the He-3 detector (left) and the cylindrical inserts that sandwich the gold foil (right); (c) Single-shell configuration of the passive NNS.

passive NNS took a total of 12 days on our departmental computing cluster, which had 5 nodes contributing a total of 123 cores.

Our GEANT4 application for generating the response functions of the passive NNS with gold-foils is provided as open-source software on GitHub [41].

2.4. Irradiation specifications

Neutron spectral measurements were performed in a radiotherapy bunker equipped with a Varian TrueBeam™ STx linac. To obtain the highest achievable neutron fluence rate, we used the 15 MV photon beam at a dose rate of 600 MU/min with the collimator jaws completely closed. The point of measurement was required to be out-of-field, to reduce photon contamination and to ensure field isotropy, but close enough to get high neutron fluence rate. Therefore, we chose our location of interest to be 1 m away from the isocenter along the treatment couch axis as shown in Fig. 3. Both the active NNS and the passive NNS were used for spectral measurements under identical experimental conditions. As the moderator configuration was altered by adding or removing moderator shells, the location of the sensitive volume was kept constant by adjusting the size of the foam platform placed underneath the NNS (an example is shown in Fig. 3). We repeated the neutron spectrum measurement three times, with both the active and passive spectrometers, to improve precision.

The measurements involving the passive NNS comprised two steps: (i) activation of the gold foils and (ii) activation analysis of the radioactive gold foils. The only stable isotope of gold (^{197}Au) may become radioactive through photon interaction (^{197}Au(γ,n)^{196}Au), or through neutron capture reactions (^{197}Au(n, γ)^{198}Au), during irradiation in our mixed field [42]. The radioactive isotopes thus created (^{196}Au and ^{198}Au) gradually decay away according to their respective half-lives, radiating characteristic photons. In the activation analysis step, these photons can be identified and distinguished using a suitable gamma-ray spectrometer, thereby enabling assessment of the neutron-induced activity.

2.5. Radioactive gold-foil analysis

We used a high-purity germanium (HPGe) detector (ORTEC DSPEC Pro; AMETEK ORTEC, Oak Ridge, TN, USA) at the SLOWPOKE reactor of Polytechnique Montréal [43] to perform spectral analysis of the radioactive gold foils within one day of foil activation. The half-life of the ^{198}Au isotope (∽2.7 days) was long enough to do the analysis the next day and was short enough to obtain statistically stable activity measurements within a reasonable time duration.

In order to determine the counting efficiency of the HPGe detector for gamma-rays with an energy of interest, the detector must be calibrated with a reference material. We used an Al-0.1% Au CRM (Certified Reference Material) foil certified by the Institute for Reference Materials and Measurements. The CRM-foil, with the same geometry as our gold-foils, was irradiated for 5 min using the SLOWPOKE reactor with a known neutron fluence rate spectrum. Using the known spectrum and Au content of the CRM-foil, and correcting for neutron self-shielding using the method described by Chilian et al. (2008) [44], we analytically determined the activity of the CRM-foil. The activated CRM foil was analysed by using the HPGe detector with MAESTRO Multichannel Analyzer Emulation Software to measure the 412 keV characteristic photons from the radioactive decay spectrum of the ^{198}Au isotope. The efficiency of the detector was thus determined for the corresponding photon energy, foil geometry and detector setting as the ratio of the number of photons counted and the calculated number of decay photons.

Our irradiated gold foils were analysed using the now-calibrated detector to count the number of characteristic photons with an uncertainty less than 1%. The activity of the gold foil saturates when the activation rate becomes equal to the decay rate of the sample [45]. Therefore, saturation activity is essentially equal to the neutron-capture rate of the gold-foil. In order to obtain the neutron-capture rate experienced by the gold foils during irradiation, the measured photon count was used to calculate the specific saturation activity (saturation activity per unit foil mass) of the gold-foil using the following equation [19,26]:

$$A_s^{\infty} = \frac{\lambda\, C\, e^{\lambda t_w}}{m\, q\, \epsilon\, (1 - e^{-\lambda t_i})\, (1 - e^{-\lambda t_m})} \tag{1}$$

Here A_s^{∞} is the specific saturation activity; m is the mass of the gold in the activated gold-foil; q is the branching ratio of the gamma-ray considered (0.955); ϵ is the detection efficiency for the corresponding gamma-ray (0.082, for our HPGe detector); λ is the decay constant of ^{198}Au isotope (2.975×10^{-6} s^{-1}); C is the net count after background and deadtime corrections. The parameters t_i, t_w & t_m are the duration of foil irradiation, the time elapsed between the end of irradiation and the start of spectral analysis, and the duration of spectral measurement, respectively.

2.6. Neutron spectral unfolding

The response functions of the passive NNS relate the calculated specific saturation activity (neutron-capture rate) of the foil to the neutron fluence rate at the location of irradiation through an integral equation of the form:

$$A_{s_i}^{\infty} = \int R_i(E)\, \Phi(E)\, dE \tag{2}$$

where $A_{s_i}^{\infty}$ is the specific saturation activity of the gold-foil used with the ith configuration of the passive NNS, $R_i(E)$ is the response function of the corresponding configuration and $\Phi(E)$ is the neutron fluence rate spectrum experienced by the gold-foil during activation.

Both the active and passive NNS have eight unique moderator configurations and hence, a set of measurements with either of these spectrometers forms a system of eight integral equations that need

Fig. 3. The passive NNS positioned at the location of measurement in our radiotherapy bunker. The black material underneath the NNS is a foam base used to maintain the central He-3 detector at a constant height.

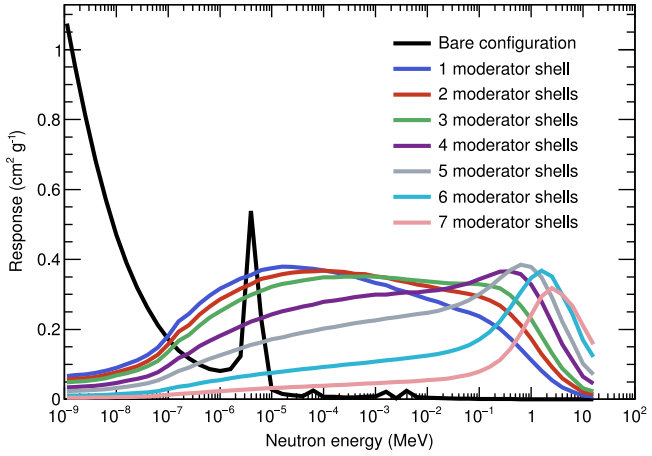

Fig. 4. Response functions of the passive NNS with gold foils, for all eight spectrometer configurations, generated through Monte Carlo simulations in GEANT4. The base configuration corresponds to the passive NNS in which no moderator shells are present and the gold foil is placed on top of the smallest insert, whereas all other configurations are represented with the number of nested shells used in the model. (For interpretation of the references to color in this figure legend, the reader is referred to the web version of this article.).

to be solved to obtain the neutron fluence rate spectrum. Our open-source MLEM-STOP algorithm [30] was used to deconvolve (unfold) the measured data with the corresponding NNS response functions. This iterative algorithm is capable of determining an optimal iteration number for which the given data set yields the optimal neutron fluence rate spectrum with the lowest noise levels achievable. We used a step function as the input guess spectrum to the algorithm, as described in our previous work [15].

Using the MLEM-STOP algorithm [30], unfolding is performed on the average of three sets of independent repeated measurements performed with each of the spectrometers. The uncertainty of the neutron fluence rate spectra for each energy bin was obtained as follows: we first defined a Gaussian distribution with the mean and standard deviation of three repeated measurements. These distributions were then sampled 100 times to obtain 100 pseudo-measurement sets, and unfolded individually. The root-mean-square (RMS) deviation of each of these unfolded spectra from the mean spectrum was then defined as the uncertainty in the corresponding energy bin, providing upper and lower uncertainty limits on the active and passive NNS spectra.

Table 1
The values of total neutron fluence rate and the ambient dose equivalent calculated from the active and passive NNS spectra.

Spectrometer	Total neutron fluence rate (cm^{-2} s^{-1})	Ambient dose equivalent (mSv h^{-1})
Active NNS	(3.831 ± 0.007) × 10^5	189.3 ± 0.4
Passive NNS	(4.2 ± 0.2) × 10^5	212.5 ± 8.7

3. Results

3.1. Response functions of the passive NNS

The set of eight response functions that were generated for our passive NNS using Monte Carlo simulations is shown in Fig. 4. It can be seen that by using all eight moderator configurations, the passive NNS sensitivity spans a sufficiently large energy range suitable for applications in radiotherapy. As anticipated, the sensitivity profile shifts to higher neutron energies with the addition of moderating material around the thermal neutron detector (gold-foil). A similar trend can be observed in the response functions of the active NNS [11].

3.2. Neutron fluence rate spectra measured using the active and passive NNS

The neutron fluence rate spectra obtained from the MLEM-STOP algorithm are shown in Fig. 5. The total neutron fluence rate and the ambient dose equivalent values were calculated from the spectra and are tabulated in Table 1. The neutron fluence rate spectrum obtained at the measurement location using the active NNS in current-mode had two predominant peaks: a large fast neutron peak around 1 MeV and a small thermal neutron peak at around 0.025 eV. The spectrum generated with the passive NNS produced peaks at the same energy bins. However, the fast neutron peak was slightly higher and the thermal peak was somewhat smaller and flatter compared to the active spectrum.

4. Discussion

The unfolded spectra from the active NNS in current-mode and the passive NNS, measured at the same location under identical experimental conditions, agree well within their uncertainties. The standard deviation of the repeated measurements for the passive NNS was relatively higher (refer Table A.2 in the Appendix), and on unfolding, this translated into a larger uncertainty for the passive NNS spectrum

Table A.2
The mean of three repeated measurements, standard deviation, and the relative standard deviation of the active and passive NNS measurements for all eight moderator configurations.

Number of moderators used in the configuration	Active NNS			Passive NNS		
	Mean of three neutron current measurements (nA)	Standard deviation (nA)	Relative standard deviation (%)	Mean of three specific saturation activity measurements (s^{-1} g^{-1})	Standard deviation (s^{-1} g^{-1})	Relative standard deviation (%)
7	0.7375	0.0004	0.06	39 405	987	2.51
6	1.334	0.002	0.17	75 038	1165	1.55
5	1.912	0.001	0.05	115 027	1996	1.74
4	1.949	0.001	0.05	125 285	3458	2.76
3	1.684	0.001	0.06	118 062	2269	1.92
2	1.4283	0.0001	0.01	108 746	2110	1.94
1	1.1024	0.0004	0.03	91 328	787	0.86
0	0.2322	0.0003	0.11	18 493	804	4.35

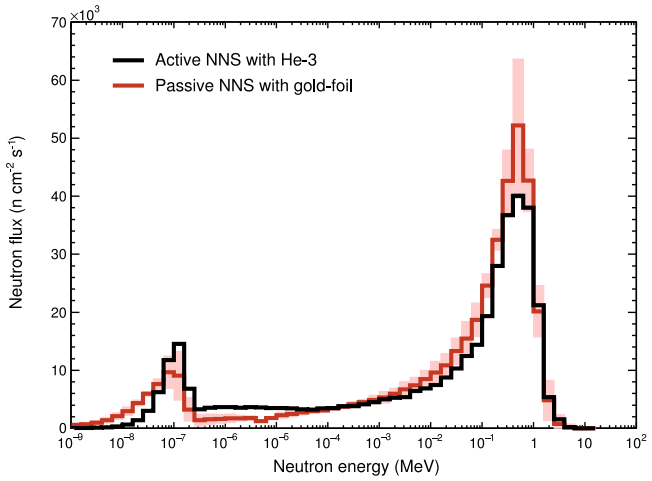

Fig. 5. Comparison of the neutron fluence rate spectra measured by the active NNS in current-mode and the passive NNS under identical experimental conditions (15 MV beam, 1 metre from the isocentre along the treatment couch). The shaded region corresponds to the uncertainty in each energy bin. (For interpretation of the references to color in this figure legend, the reader is referred to the web version of this article.).

compared to that of the active NNS. It is important to note that the reported uncertainties only take into account the statistical (type A) uncertainty, but there are other sources of potential systematic (type B) uncertainty including foil non-uniformity, foil purity, foil positioning and foil-to-foil variations. Below, we discuss some of the factors that may have contributed to the type B uncertainties of the active and passive NNS spectra.

The He-3 detector of the active NNS occupies ∽500 times more volume than the gold foil disc inside the nested moderators. Therefore, the volume averaging effect for the He-3 detector is much higher and hence it is less susceptible to random variations in the neutron field between irradiations and to the effects of small positional changes of the detector. This partially explains why the active NNS has more precision compared to the passive system with gold foils. The response functions for the active system were generated using detailed modelling of the detector and moderators, although small deviations in its response from the simulation model may exist due to manufacturing variabilities. However, the vendor provides a normalization factor obtained during calibration for every active NNS to account for these deviations. Similarly, in the case of a passive NNS with gold foils, the foils themselves may have non-uniformities in thickness, density and other defects that may have caused system responses different to those described by our model. Obtaining a normalization factor, to account for the gold foil variabilities, with a similar approach to that of He-3 is not feasible as the low flux of a calibration neutron source would require prohibitively-long measurement durations. Hence, this inability to correct for deviations of the system from ideal behaviour factors into the type B uncertainty.

Despite the various uncertainties, the active and passive spectra agree well, and their agreement serves as experimental validation of the use of the active NNS in current-mode under high neutron fluence rate conditions.

Although the passive NNS eliminates the need to perform separate irradiations to isolate the neutron contribution from the photon contamination, a passive system is not ideal for frequent neutron spectrometry in radiotherapy. The neutron fluence rate from a medical linac, although high, is not ample enough for the rapid activation of a gold foil. The time required to perform one complete set of irradiations with the passive NNS was ∽8 times longer than that with the active NNS in current-mode. For example, we had to irradiate the passive bare configuration (the least sensitive configuration) for 30 min to obtain a detectable foil activity. It was hence not feasible to perform all three repeated measurements on the same day with the passive NNS, whereas the active NNS was able to achieve three repeated measurements in under an hour. Similarly, it is not practical to obtain measurements at locations more distant from the linac due to the inverse-square dependency of fluence on distance.

Additionally, the user must generate new response functions for the passive NNS every time the foil characteristics (thickness, density, purity etc.) are changed whereas with the active NNS, normalizing a new He-3 detector eliminates the need to generate new system response functions. For these reasons, we only recommend our passive NNS for validation of similar active neutron spectrometers, not for routine use.

5. Conclusion

We have developed a passive NNS incorporating gold foils and used it to validate the accuracy of an active NNS in current-mode under the high neutron fluence rate conditions of a high-energy radiotherapy linac. This included the development of a modelling and experimental workflow for using the passive NNS for spectral measurements. Comparison of the spectra measured with the active NNS and the passive NNS showed good agreement, which serves as validation of the use of the active NNS in current-mode in high neutron fluence rate environments.

CRediT authorship contribution statement

Felix Mathew: Methodology, Software, Validation, Formal analysis, Investigation, Writing - original draft. **Cornelia Chilian:** Methodology, Formal analysis, Resources, Writing - review & editing. **Logan Montgomery:** Software, Writing - review & editing, Supervision. **John Kildea:** Conceptualization, Resources, Writing - review & editing, Supervision, Project administration, Funding acquisition.

Declaration of competing interest

The authors declare that they have no known competing financial interests or personal relationships that could have appeared to influence the work reported in this paper.

Acknowledgements

We acknowledge the support provided by the Natural Sciences and Engineering Research Council of Canada (NSERC) through a Discovery Grant (John Kildea) and the CREATE Medical Physics Research Training Network grant (Grant number: 432290). Partial support for this research was provided by the Canadian Nuclear Safety Commission (CNSC). We gratefully appreciate the insights and support of Jacques Dubeau (Detec Inc.) and Michael Evans (Radiation Safety Officer, Cedars Cancer Centre), and Chris Lund for valuable discussions regarding the implementation and programming details.

Appendix

Table A.2 shows the mean value of three repeated measurements obtained using the active NNS in current-mode and the passive NNS for each of their eight moderator configurations. The mean neutron current and the mean saturation activity were used to unfold the neutron fluence rate spectra. The standard deviation and the relative standard deviation of the measurements are also tabulated.

References

[1] A. Śladowska, Modern External Beam Radiotherapy techniques–Intensity modulated radiotherapy, Acta Phys. Polon. A 115 (2) (2009) 586–590, http://dx.doi.org/10.12693/aphyspola.115.586.

[2] H. Vega-Carrillo, S. Martinez-Ovalle, A. Lallena, G. Mercado, J. Benites-Rengifo, Neutron and photon spectra in LINACs, Appl. Radiat. Isot. 71 (2012) 75–80, http://dx.doi.org/10.1016/j.apradiso.2012.03.034.

[3] T. Fujibuchi, S. Obara, H. Sato, M. Nakajima, N. Kitamura, T. Sato, H. Kumada, T. Sakae, T. Fujisaki, Estimate of Photonuclear Reaction in a Medical linear Accelerator using a water-equivalent Phantom, Prog. Nucl. Sci. Technol. 2 (2011) 803–807, http://dx.doi.org/10.15669/pnst.2.803.

[4] S.F. Kry, U. Titt, F. Pönisch, O.N. Vassiliev, M. Salehpour, M. Gillin, R. Mohan, Reduced neutron production through use of a Flattening-Filter–Free accelerator, Int. J. Radiat. Oncol. Biol. Phys. 68 (4) (2007) 1260–1264, http://dx.doi.org/10.1016/j.ijrobp.2007.04.002.

[5] F. Sanchez, G. Madurga, R. Arráns, Neutron measurements around an 18 MV linac, Radiother. Oncol. 15 (3) (1989) 259–265, http://dx.doi.org/10.1016/0167-8140(89)90094-7.

[6] M.R. Expósito, B. Sánchez-Nieto, J.A. Terrón, C. Domingo, F. Gómez, F. Sánchez-Doblado, Neutron contamination in radiotherapy: Estimation of second cancers based on measurements in 1377 patients, Radiother. Oncol. 107 (2) (2013) 234–241, http://dx.doi.org/10.1016/j.radonc.2013.03.011.

[7] R. Takam, E. Bezak, L. Marcu, E. Yeoh, Out-of-field neutron and leakage photon exposures and the associated risk of second cancers in high-Energy Photon Radiotherapy: Current status, Radiat. Res. 176 (4) (2011) 508–520, http://dx.doi.org/10.1667/rr2606.1.

[8] A. Ottolenghi, V. Smyth, K. Trott, Assessment of cancer risk from neutron exposure–The ANDANTE project, Radiat. Meas. 57 (2013) 68–73, http://dx.doi.org/10.1016/j.radmeas.2012.10.017.

[9] G. Baiocco, S. Barbieri, G. Babini, J. Morini, D. Alloni, W. Friedland, P. Kundrát, E. Schmitt, M. Puchalska, L. Sihver, et al., The origin of neutron biological effectiveness as a function of energy, Sci. Rep. 6 (2016) 34033, http://dx.doi.org/10.1038/srep34033.

[10] J. Valentin, Relative biological effectiveness (RBE), quality factor (Q), and radiation weighting factor (wR): ICRP Publication 92, Ann. ICRP 33 (4) (2003) 1–121, http://dx.doi.org/10.1016/s0146-6453(03)00024-1.

[11] J. Dubeau, S. Hakmana Witharana, J. Atanackovic, A. Yonkeu, J. Archambault, A neutron spectrometer using nested moderators, Radiat. Prot. Dosim. 150 (2) (2012) 217–222, http://dx.doi.org/10.1093/rpd/ncr381.

[12] R.L. Bramblett, R.I. Ewing, T. Bonner, A new type of neutron spectrometer, Nucl. Instrum. Methods 9 (1) (1960) 1–12, http://dx.doi.org/10.1016/0029-554X(60)90043-4.

[13] H. Ing, T. Clifford, T. McLean, W. Webb, T. Cousins, J. Dhermain, ROSPEC-A simple reliable high resolution neutron spectrometer, Radiat. Prot. Dosim. 70 (1–4) (1997) 273–278, http://dx.doi.org/10.1093/oxfordjournals.rpd.a031959.

[14] M. Das, B. Chatterjee, B. Roy, S. Roy, Superheated drop as a neutron spectrometer, Nucl. Instrum. Methods Phys. Res. A 452 (1–2) (2000) 273–279, http://dx.doi.org/10.1016/S0168-9002(00)00423-X.

[15] R. Maglieri, A. Licea, M. Evans, J. Seuntjens, J. Kildea, Measuring neutron spectra in radiotherapy using the nested neutron spectrometer, Med. Phys. 42 (11) (2015) 6162–6169, http://dx.doi.org/10.1118/1.4931963.

[16] M. Hagiwara, T. Sanami, Y. Iwamoto, H. Arakawa, N. Shigyo, N. Mokhov, A. Leveling, D. Boehnlein, V. Kamran, T. Nakamura, et al., Shielding experiments at high energy accelerators of Fermilab (III): neutron spectrum measurements in Intense pulsed neutron fields of the 120-GeV proton facility using A current Bonner Sphere Technique, Prog. Nucl. Sci. Technol. 5 (2011) 9, http://dx.doi.org/10.15669/pnst.1.52.

[17] International Organization for Standardization, Neutron Reference Radiations for Calibrating Neutron-measuring Devices Used for Radiation Protection Purposes and for Determining Their Response as a Function of Neutron Energy, ISO, 1989.

[18] IAEA, Safety Report Series No. 16, Calibration of Radiation Protection Monitoring Instruments, IAEA Vienna, 2000.

[19] K. Amgarou, V. Lacoste, H. Muller, F. Fernández, Set-up of a passive Bonner sphere system for neutron spectrometry at mixed fields with predominant photon component based on activation detector, Radiat. Prot. Dosim. 126 (1–4) (2007) 337–341, http://dx.doi.org/10.1093/rpd/ncm070.

[20] R. Bedogni, P. Ferrari, G. Gualdrini, A. Esposito, Design and experimental validation of a Bonner Sphere Spectrometer based on Dysprosium activation foils, Radiat. Meas. 45 (10) (2010) 1201–1204, http://dx.doi.org/10.1016/j.radmeas.2010.04.005.

[21] P. Vlk, M. Pavlovič, Calculation and validation of the response matrix for a neutron multisphere Spectrometer with an Indium Central Detector, Radiat. Prot. Dosim. 179 (1) (2018) 1–8, http://dx.doi.org/10.1093/rpd/ncx183.

[22] Z. Wang, R.M. Howell, S.F. Kry, E.A. Burgett, N.E. Hertel, M. Salehpour, Characterization of a Gold-and-Indium Dual-Activation-Foil-based Bonner Sphere System, Nucl. Technol. 168 (3) (2009) 603–609, http://dx.doi.org/10.13182/NT09-A9276.

[23] A. Asuncion-Astronomo, F.C. Hila, C.A.M. Dingle, C.V. Balderas, R.M.M.D. Cruz, N.R.D. Guillermo, Design of a multi-shell portable neutron spectrometry system based on indium foil detectors, Radiat. Meas. 132 (2020) 106248, http://dx.doi.org/10.1016/j.radmeas.2020.106248.

[24] E. Vagena, K. Theodorou, S. Stoulos, Thick-foils activation technique for neutron spectrum unfolding with the MINUIT routine—comparison with GEANT4 simulations, Nucl. Instrum. Methods Phys. Res. A 887 (2018) 64–69, http://dx.doi.org/10.1016/j.nima.2018.01.025.

[25] F. Fernández, C. Domingo, K. Amgarou, J. Castelo, T. Bouassoule, M. Garcia, E. Luguera, Neutron measurements in a Varian 2100c LINAC facility using a Bonner sphere system based on passive gold activation detectors, Radiat. Prot. Dosim. 126 (1–4) (2007) 361–365, http://dx.doi.org/10.1093/rpd/ncm075.

[26] K. Amgarou, V. Lacoste, A. Martin, B. Asselineau, L. Donadille, Neutron spectrometry with a passive Bonner sphere system Around a medical LINAC and evaluation of the associated unfolding uncertainties, IEEE Trans. Nucl. Sci. 56 (5) (2009) 2885–2895, http://dx.doi.org/10.1109/TNS.2009.2026416.

[27] D. Thomas, A. Bardell, E. Macaulay, Characterisation of a gold foil-based Bonner sphere set and measurements of neutron spectra at a medical accelerator, Nucl. Instrum. Methods Phys. Res. A 476 (1–2) (2002) 31–35, http://dx.doi.org/10.1016/S0168-9002(01)01384-5.

[28] D. Thomas, N. Hawkes, L. Jones, P. Kolkowski, N. Roberts, Characterization and utilization of a Bonner sphere set based on gold activation foils, Radiat. Prot. Dosim. 126 (1–4) (2007) 229–233, http://dx.doi.org/10.1093/rpd/ncm047.

[29] L. Montgomery, M. Evans, L. Liang, R. Maglieri, J. Kildea, The effect of the flattening filter on photoneutron production at 10 MV in the Varian TrueBeam linear accelerator, Med. Phys. 45 (10) (2018) 4711–4719, http://dx.doi.org/10.1002/mp.13148.

[30] L. Montgomery, A. Landry, G. Al Makdessi, F. Mathew, J. Kildea, A novel MLEM stopping criterion for unfolding neutron fluence spectra in radiation therapy, Nucl. Instrum. Methods Phys. Res. A (2020) 163400, http://dx.doi.org/10.1016/j.nima.2020.163400.

[31] J. Apostolakis, D.H. Wright, G. Collaboration, An overview of the GEANT4 toolkit, in: AIP Conference Proceedings, Vol. 896, American Institute of Physics, 2007, pp. 1–10, http://dx.doi.org/10.1063/1.2720452.

[32] S. Agostinelli, J. Allison, K.a. Amako, J. Apostolakis, H. Araujo, P. Arce, M. Asai, D. Axen, S. Banerjee, G. Barrand, et al., GEANT4—a simulation toolkit, Nucl. Instrum. Methods Phys. Res. A 506 (3) (2003) 250–303, http://dx.doi.org/10.1016/S0168-9002(03)01368-8.

[33] J. Allison, K. Amako, J. Apostolakis, H. Araujo, et al., Geant4 developments and applications, IEEE Trans. Nucl. Sci. 53 (2003) 270–278, http://dx.doi.org/10.1109/TNS.2006.869826.

[34] J. Allison, K. Amako, J. Apostolakis, P. Arce, M. Asai, T. Aso, et al., Recent developments in Geant4, Nucl. Instrum. Methods Phys. Res. A 835 (2016) 186–225, http://dx.doi.org/10.1016/j.nima.2016.06.125.

[35] M. Herman, ENDF-6 Formats Manual Data Formats and Procedures for the Evaluated Nuclear Data File ENDF/B-VI and ENDF/B-VII, Technical Report, Brookhaven National Laboratory (BNL) National Nuclear Data Center, 2009, http://dx.doi.org/10.2172/981813.

[36] E. Mendoza, D. Cano-Ott, C. Guerrero, R. Capote, New Evaluated Neutron Cross Section Libraries for the GEANT4 Code, Technical Report, International Atomic Energy Agency, 2012.
[37] E. Mendoza, D. Cano-Ott, T. Koi, C. Guerrero, New standard evaluated neutron cross section libraries for the GEANT4 code and first verification, IEEE Trans. Nucl. Sci. 61 (4) (2014) 2357–2364, http://dx.doi.org/10.1109/tns.2014.2335538.
[38] D. Rogers, A. Bielajew, Monte Carlo techniques of electron and Photon Transport for Radiation dosimetry, Dosim. Ioniz. Radiat. 3 (1990) 427–539, http://dx.doi.org/10.1016/B978-0-12-400403-0.50009-9.
[39] B. James, Variance reduction techniques, J. Oper. Res. Soc. 36 (6) (1985) 525–530, http://dx.doi.org/10.2307/2582825.
[40] K. Amgarou, V. Lacoste, Response matrix evaluations of a passive Bonner sphere system used for neutron spectrometry at pulsed, intense and complex mixed fields, J. Instrum. 5 (09) (2010) P09002, http://dx.doi.org/10.1088/1748-0221/5/09/P09002.
[41] F. Mathew, GitHub repository of the software - Passive_NNS_with_gold-foil–Response_function_generator: First release of the response function generator, 2020, http://dx.doi.org/10.5281/zenodo.3742354.
[42] K. Haddad, O. Anjak, B. Yousef, Neutron and high energy photon fluence estimation in CLINAC using gold activation foils, Rep. Pract. Oncol. Radiother. 24 (1) (2019) 41–46, http://dx.doi.org/10.1016/j.rpor.2018.08.009.
[43] G. Kennedy, J. St-Pierre, The neutron activation analysis laboratory at the Ecole Polytechnique de Montreal, J. Radioanal. Nucl. Chem. 180 (2) (1994) 347–351, http://dx.doi.org/10.1007/bf02035926.
[44] C. Chilian, J. St-Pierre, G. Kennedy, Complete thermal and epithermal neutron self-shielding corrections for NAA using a spreadsheet, J. Radioanal. Nucl. Chem. 278 (3) (2008) 745–749.
[45] H.E. Johns, J.R. Cunningham, The Physics of Radiology, Charles C. Thomas Springfield, IL, 1983, http://dx.doi.org/10.1118/1.595545.